Giazotto, Francesco; Heikkilä, Tero; Pepe, Giovanni; Helistö, Panu; Luukanen, Antti; Pekola, Jukka

Ultrasensitive proximity Josephson sensor with kinetic inductance readout

Published in:
Applied Physics Letters

DOI:
10.1063/1.2908922

Published: 01/01/2008

Document Version
Publisher's PDF, also known as Version of record

Ultrasensitive proximity Josephson sensor with kinetic inductance readout

Francesco Giazotto' , Tero T. Heikkilä, Giovanni Piero Pepe, Panu Helistö, Arttu Luukanen, and Jukka P. Pekola

Citation: Appl. Phys. Lett. **92**, 162507 (2008); doi: 10.1063/1.2908922
View online: http://dx.doi.org/10.1063/1.2908922
View Table of Contents: http://aip.scitation.org/toc/apl/92/16
Published by the American Institute of Physics

Ultrasensitive proximity Josephson sensor with kinetic inductance readout

Francesco Giazotto,[1,a] Tero T. Heikkilä,[2] Giovanni Piero Pepe,[3] Panu Helistö,[4] Arttu Luukanen,[5] and Jukka P. Pekola[2]
[1]*NEST CNR-INFM and Scuola Normale Superiore, I-56126 Pisa, Italy*
[2]*Low Temperature Laboratory, Helsinki University of Technology, P.O. Box 3500, FIN-02015 TKK, Finland*
[3]*CNR-INFM Coherentia and Dipartimento Scienze Fisiche, Università di Napoli "Federico II," Monte Sant'Angelo, I-80125 Napoli, Italy*
[4]*VTT Information Technology, Tietotie 3, Fin-02150 Espoo, Finland*
[5]*Millilab, VTT, Tietotie 3, Fin-02150 Espoo, Finland*

(Received 18 February 2008; accepted 24 March 2008; published online 22 April 2008)

We propose a mesoscopic kinetic-inductance radiation detector based on a long superconductor-normal metal-superconductor Josephson junction. The operation of this proximity Josephson sensor relies on large kinetic inductance variations under irradiation due to the exponential temperature dependence of the critical current. Coupled with a dc superconducting quantum interference device readout, the PJS is able to provide a signal to noise (S/N) ratio up to $\sim 10^3$ in the terahertz regime if operated as calorimeter, while electrical noise equivalent power as low as $\sim 7\times 10^{-20}$ W/$\sqrt{\text{Hz}}$ at 200 mK can be achieved in the bolometer operation. The high performance together with the ease of fabrication make this structure attractive as an ultrasensitive cryogenic detector of terahertz electromagnetic radiation. © *2008 American Institute of Physics*. [DOI: 10.1063/1.2908922]

Superconducting single-photon detectors[1–3] offer high infrared detection efficiency, high-speed timing resolution, and few-nanosecond reset times. They have been applied in several fields including spectroscopy of ultrafast quantum phenomena,[4] optical communications,[5] quantum cryptography,[6] and fast digital circuit testing.[7] On the other hand, a wide potential for superconducting nanoscale detectors used as advanced bolometers is also expected in several astrophysical space applications, where bolometers are promising candidates to meet future needs of cooled telescopes. The interest lies in the negligible Johnson noise they show with a noise equivalent power (NEP) as low as 10^{-18} W/$\sqrt{\text{Hz}}$. Hot-electron resistive microbolometers and kinetic inductance superconducting detectors (KIDs) represent high performance devices able to reach NEP $\lesssim 10^{-19}$ W/$\sqrt{\text{Hz}}$ at $T \geqslant 1$ K.[8] KIDs (Refs. 9) offer about the same NEP and response time as resistive bolometers and hot electron detectors, and they can operate at temperatures much below the critical temperature where the generation-recombination noise is small.

Here, we propose a KID based on a long superconductor-normal metal-superconductor Josephson junction. It exploits large kinetic inductance variations under irradiation thanks to the exponential temperature dependence of the supercurrent, and yields a high signal-to-noise (S/N) ratio ($\sim 10^3$ around 40 THz) and a low NEP ($\sim 7\times 10^{-20}$ W/$\sqrt{\text{Hz}}$ at 200 mK). The ease of implementation combined with large array scalability make this structure promising as a sub-Kelvin ultrasensitive detector of far- and midinfrared electromagnetic radiations.

The structure we envision is sketched in Fig. 1(a) and consists of a diffusive normal metal (N) wire of length l coupled to two superconducting leads (S) through transparent contacts, thus realizing a *SNS* Josephson weak link. An antenna eventually couples the incident radiation to the N wire. We assume that the Josephson junction is long, i.e., $\Delta \gg \hbar D/l^2 = E_{\text{Th}}$, where Δ is the S gap, D is the diffusion coefficient of N, and E_{Th} is the Thouless energy. The radiation coupled to the junction heats the electrons in N to temperature T_e. For $E_{\text{Th}} \ll k_B T_e \ll \Delta$, the Josephson current is $I_J = I_c \sin(\phi)$, where ϕ is the phase difference across superconductors and[10]

$$I_c = \frac{64\pi k_B T_e}{(3+2\sqrt{2})eR_N}\sqrt{\frac{2\pi k_B T_e}{E_{\text{Th}}}}\exp\left(-\sqrt{\frac{2\pi k_B T_e}{E_{\text{Th}}}}\right) \qquad (1)$$

is the junction critical current. Hence, in this limit, I_c exponentially depends on the electron temperature and is independent of the phonon temperature T_{bath}. In Eq. (1), $R_N = \rho l/\mathcal{A}$ is the normal-state resistance of the junction, $\rho = (\nu_F e^2 D)^{-1}$ is the wire resistivity, $\mathcal{A}$ its cross section, and ν_F is the density of states at the Fermi level in N. For our simulation, we choose a 10-nm-thick silver (Ag) wire with $l = 1$ μm, width of 100 nm (volume $\Omega = 10^{-21}$ m^3), $\nu_F = 1.0\times 10^{47}$ J^{-1} m^{-3}, and $D = 0.01$ m^2 s^{-1}. With the aforementioned parameters $R_N \simeq 38$ Ω and $E_{\text{Th}} \simeq 6.6$ μeV. By choosing, for instance, Nb as S electrodes ($\Delta = 1.52$ meV) we get $\Delta/E_{\text{Th}} \simeq 230$, thus providing the frame of the *long* junction limit. The critical current I_c versus T_e is shown in Fig. 1(b) for $\phi = \pi/2$ and $\Delta/E_{\text{Th}} = 230$ (dashed line). In our case, I_c saturates around 1.7 μA at $T_e \simeq 50$ mK and is suppressed by a factor of ~ 20 at 1 K due to the exponential dependence on T_e. For a comparison, the approximated result from Eq. (1) is also shown (full line) and will be used in the following. Such suppression of I_c produces a large enhancement of the junction kinetic inductance $L_k = \hbar/(2eI_c)$. Measuring L_k variations with a suitable readout scheme allows us to accurately detect the radiation absorbed by the *SNS* junction.

In order to understand the operation principle of the proximity Josephson sensor (PJS) as a calorimeter (i.e., in pulsed excitation operation) as well as a bolometer (i.e., in continuous excitation operation), it is useful to consider the inset of Fig. 1(b), which shows a sketch of time evolution of T_e in N after the arrival of a photon. We assume that T_e is

[a]Author to whom correspondence should be addressed. Electronic mail: giazotto@sns.it.

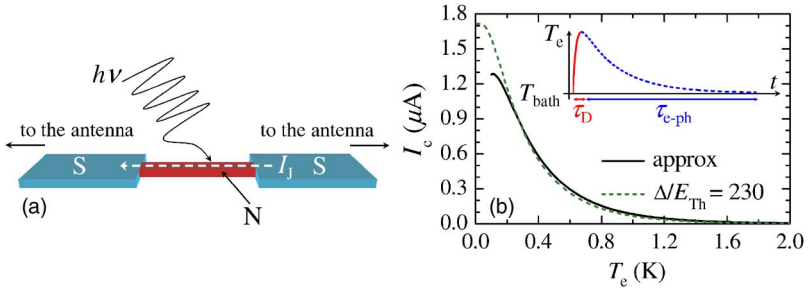

FIG. 1. (Color online) (a) Scheme of the PJS. Incident electromagnetic radiation elevates the electron temperature (T_e) in the N wire, thus strongly suppressing the Josephson current. This leads to a large enhancement of the junction kinetic inductance. (b) Supercurrent I_c vs electron temperature T_e of a long *SNS* Josephson junction calculated at $\phi=\pi/2$ from Eq. (1) (full line) and for $\Delta/E_{Th}=230$ (dashed line). The inset shows a sketch of time evolution of T_e after absorption of radiation (see text).

elevated with respect to T_{bath}, depending on the energy of the impinging photon and uniformly along N, over a time scale set by the diffusion time $\tau_D=l^2/D$ [see the red line in the inset of Fig. 1(b)]. With our parameters $\tau_D=10^{-10}$ s. Then, after the absorption of a photon, T_e relaxes toward T_{bath} over a time scale set by the electron-phonon interaction time ($\tau_{e\text{-ph}}$), given by $\tau_{e\text{-ph}}=1/(\alpha T_{bath}^3)$,[11] where $\alpha\approx 0.34\Sigma/(k_B^2\nu_F)$, and Σ is the electron-phonon coupling constant. By setting $\Sigma=5\times10^8$ W m^{-3} K^{-5}, as appropriate for Ag,[11] $\tau_{e\text{-ph}}\sim 1\times10^{-4}\cdots1\times10^{-7}$ s in the $0.1\cdots1.0$ K temperature range so that $\tau_{e\text{-ph}}\gg\tau_D$ [see the blue line in the inset of Fig. 1(b)].

In the pulsed mode, after the arrival of a photon of frequency ν at time $t=0$, the electron temperature in N can be determined by solving the heat equation $C_e(\partial T_e/\partial t)=P_{opt}$,[11] where $C_e=(\pi^2\nu_F k_B^2 T_e)/3$ is the electron heat capacity, and $P_{opt}=(2\pi\hbar\nu/\Omega)\delta(t)$ is the optical input power per volume per incident photon. In writing the heat equation, we neglected the spatial dependence of T_e in N, as well as the interaction with the lattice phonons, the latter occurring on a time scale $\tau_{e\text{-ph}}\gg\tau_D$. Solving the heat equation, we get $T_e(\nu)=\sqrt{T_{bath}^2+12\hbar\nu/(\pi\Omega\nu_F k_B^2)}$, which shows that small N volumes are required to achieve large enhancement of T_e. This condition can be easily met in metallic *SNS* junctions, where N island with volumes below 10^{-21} m^3 can be routinely fabricated with the present technology. The relative variation of the kinetic inductance, $\delta L_k/L_k^0=[L_k(\nu)-L_k(0)]/L_k(0)$ is displayed in Fig. 2(a) as a function of ν at different T_{bath}. In the present structure, $\delta L_k/L_k^0$ of about 14% for 1 THz photon and around 163% for 10 THz photon can be achieved at 200 mK. At higher bath temperatures, $\delta L_k/L_k^0$ is reduced to about 3% at 1 THz and around 35% at 10 THz at $T_{bath}=1$ K. Such kinetic inductance variations allow for a very large signal to noise ratio for single-photon detection.

The PJS operation in continuous excitation can be described by considering those mechanisms which drive power into the N electrons. At low temperature (typically below 1 K), the main contribution in metals is related to electron-phonon heat flux, which can be modeled by $\dot{Q}_{e\text{-ph}}=\Sigma\Omega(T_e^5-T_{bath}^5)$.[11] The steady-state T_e under irradiation with a continuous power P_{opt} thus directly follows from the solution of the energy balance equation $P_{opt}+\dot{Q}_{e\text{-ph}}=0$, which gives $T_e(P_{opt})=\sqrt[5]{(P_{opt}/\Sigma\Omega)+T_{bath}^5}$. This expression shows that both reduced Ω and small Σ are required to maximize T_e enhancement upon power irradiation. The impact of continuous power excitation on the junction kinetic inductance is shown in Fig. 2(b), which shows $\delta L_k/L_k^0=[L_k(P_{opt})-L_k(0)]/L_k(0)$ versus P_{opt} at several T_{bath}. Notably, $\delta L_k/L_k^0$ as large as $\simeq$130% for $P_{opt}=10$ fW and $\simeq$2000% for $P_{opt}=1$ pW at $T_{bath}=0.2$ K can be achieved. At higher bath temperatures, $\delta L_k/L_k^0$ gets reduced, reaching values of $\simeq$1% for $P_{opt}=10$ fW and $\simeq$100% for $P_{opt}=1$ pW at 1 K.

We now turn on discussing the PJS performance by considering a superconducting quantum interference device (SQUID) readout, as shown in Fig. 3(a).[12] A constant bias current I_b divides into two parts, i.e., one flowing through the *SNS* junction,[13] and the other (I_L) through a load inductor (L) coupled to a dc SQUID. Upon irradiation, an enhancement of L_k results in a variation of I_L, thus producing a magnetic field which is detected by the SQUID. The magnetic flux generated by the incident radiation is given by $\Phi=MI_L$, where M is the mutual inductance between the SQUID and the *SNS* junction loop. In the linearized regime, i.e., by assuming $LI_L\ll\Phi_0$, where Φ_0 is the flux quantum, we get $I_L\approx I_b\Phi_0/(\Phi_0+LI_c)$, and $dI_L/dI_c\approx LI_b\Phi_0/(\Phi_0+LI_c)^2$. In the pulsed detection mode, the S/N ratio is

$$\frac{S}{N}=\frac{(d\Phi/dT_e)\delta T_e}{\delta\Phi_n\sqrt{\omega}}=\left|\frac{M(dI_L/dI_c)(dI_c/dT_e)\delta T_e}{\delta\Phi_n\sqrt{\omega}}\right|, \qquad (2)$$

where $\delta\Phi_n$ is the flux sensitivity of the dc SQUID and ω its bandwidth. The S/N ratio versus ν is shown in Fig. 3(b) at different T_{bath}. Here, we set $L=100$ nH, $M=10$ nH, $\omega=1$ MHz, $\delta\Phi_n=10^{-7}\Phi_0/\sqrt{\text{Hz}}$,[14] and $I_b=0.8I_c(\nu)$. Notably, very high S/N ratios can be achieved with the *PJS* in the 100 GHz–100 THz frequency range. The S/N ratio is maxi-

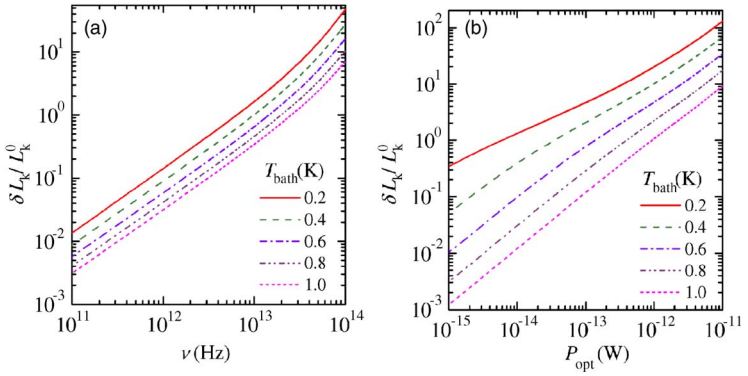

FIG. 2. (Color online) (a) $\delta L_k/L_k^0$ vs ν at different T_{bath}. (b) $\delta L_k/L_k^0$ vs P_{opt} calculated at different T_{bath}.

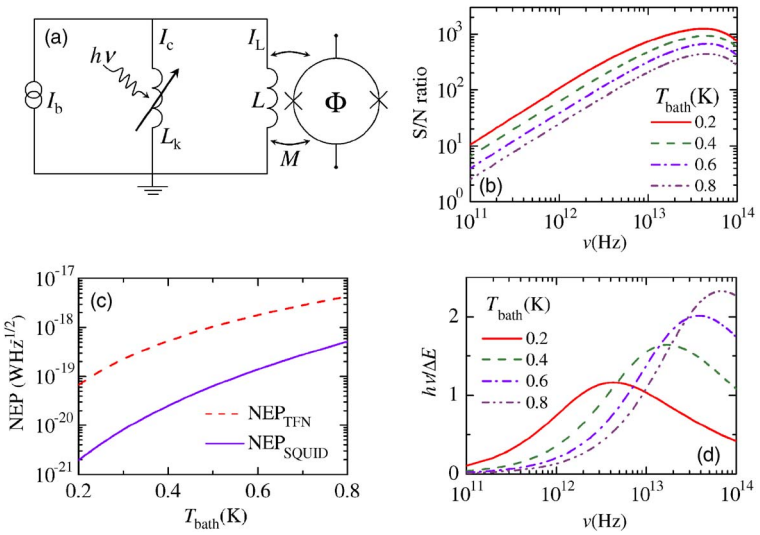

FIG. 3. (Color online) (a) Scheme of the KID with a dc SQUID readout. (b) S/N ratio vs ν calculated at different T_{bath}. (c) Temperature dependencies of NEP due to thermal fluctuation noise (TFN) and to the SQUID readout. (d) Resolving power vs ν calculated at different T_{bath}.

mized around 40 THz where it obtains values of $\sim 1.2 \times 10^3$ at $T_{bath}=0.2$ K. In the bolometer operation, on the other hand, an important figure of merit is the NEP, which is due to several uncorrelated noise sources. In our case, the dominant contribution is due to thermal fluctuation noise-limited NEP (NEP$_{TFN}$), given by NEP$_{TFN}=\sqrt{5k_B\Sigma\Omega(T_e^6+T_{bath}^6)}$,[11] while the contribution due to Johnson noise is absent, thanks to the operation of the junction in the dissipationless regime. The contribution of the SQUID readout to NEP (NEP$_{SQUID}$) can be determined by setting S/N=1, $\omega=1$ Hz, and solving Eq. (2) for P_{opt}. Figure 3(c) shows the NEP$_{TFN}$ (dashed line) and NEP$_{SQUID}$ (full line) versus T_{bath}. NEP$_{SQUID}$ is significantly smaller than NEP$_{TFN}$, and the latter can be as low as $\simeq 7 \times 10^{-20}$ W/$\sqrt{\text{Hz}}$ at 0.2 K. Further reduction of NEP$_{TFN}$ is possible by lowering Ω as well as by exploiting materials with lower Σ. Above, we have discussed the electrical NEP—the optical NEP is of the same order of magnitude. This is because the resistance of the device can be easily matched to common broadband self-similar lithographic antennas. The PJS resolving power ($2\pi\hbar\nu/\Delta E$) versus frequency, where $\Delta E \approx 2\sqrt{2\ln 2}\text{NEP}_{TFN}(\nu)\sqrt{\tau_{e\text{-ph}}}$ is the energy resolution of full width at half maximum,[11] is displayed in Fig. 3(d) for different T_{bath}. In particular, the figure shows that resolving power values between ~ 1.2 and ~ 2.3 can be achieved in the $5\cdots 70$ THz frequency range for $T_{bath} \gtrsim 400$ mK, thus making the PJS suitable for *far-* and *midinfrared* single-photon detection.

The mechanism for the supercurrent in *SNS* junctions is due to the proximity effect, giving rise in the N local density of states to an energy minigap of size $E_g=c(\phi)E_{Th}$, with $c(0)\approx 3.1$,[15] which we have ignored in the expressions for the heat capacity and electron-phonon coupling. Due to the minigap, both of these quantities are reduced inside the *N* wire, further improving the device resolution.

In summary, we have analyzed a PJS based on a long *SNS* junction in the kinetic inductance mode. S/N ratio as high as $\sim 10^3$ and NEP below 10^{-19} W/$\sqrt{\text{Hz}}$ at 0.2 K have been found to be achievable. Together with the available resolving power, the PJS is a promising candidate for single-photon detection in the terahertz regime.

The authors thank the NanoSciERA "NanoFridge" project and the Academy of Finland for financial support. This work has been partially supported by MIUR, PRIN 2006, under the project Macroscopic Quantum Systems-Fundamental Aspects and Applications of Non Conventional Josephson Structures.

[1] A.J. Kerman, E. A. Dauler, W. E. Keicher, J. K. W.Yang, K. K Berggren, G. N Gol'tsman, and B. M. Voronov, Appl. Phys. Lett. **88**, 111116 (2006).
[2] G. Gol'tsman, O. Okunev, G. Chulkova, A. Lipatov, A. Dzardanov, K. Smirnov, A. Semenov, B. Voronov, C. Williams, and R. Sobolewski, IEEE Trans. Appl. Supercond. **11**, 574 (2001).
[3] A. A Houck, D. I. Schuster, J. M. Gambetta, J. A Schreier, B. R. Johnson, J. M. Chow, L. Frunzio, J. Majer, M. H. Devoret, S. M Girvin, and R. J. Schoelkopf, Nature (London) **449**, 328 (2007).
[4] M. A. Jaspan, J. L. Habif, R. H. Hadfield, and S. W. Nam, Appl. Phys. Lett. **89**, 031112 (2006).
[5] S. Robinson, A. J. Kerman, E. A. Dauler, R. J. Barron, D. O. Caplan, M. L. Stevens, J. J. Carney, S. A. Hamilton, J. K. W. Yang, and K. K. Berggren, Opt. Lett. **31**, 444 (2006).
[6] S. Benjamin, Science **290**, 2273 (2000).
[7] A. Korneev, A. Lipatov, O. Okunev, G. Chulkova, K. Smirnov, G. Gol'tsman, J. Zhang, W. Slysz, A. Verevkin, and R. Sobolewski, Microelectron. Eng. **69**, 274 (2003).
[8] A. V. Sergeev, V. V. Mitin, and B. S. Karasik, Appl. Phys. Lett. **80**, 817 (2002); J. J. Bock, J. Glenn, S. M. Grannan, K. D. Irwin, A. E. Lange, H. G. LeDuc, and A. D. Turner, Proc. SPIE **3357**, 297 (1998).
[9] N. Grossman, D. G. McDonald, and J. E. Sauvageau, IEEE Trans. Magn. **27**, 2677 (1991); N. Bluzer and M. G. Forrester, Opt. Eng. **33**, 697 (1994).
[10] A. D. Zaikin and G. F. Zharkov, Sov. J. Low Temp. Phys. **7**, 184 (1981); F. K. Wilhelm, A. D. Zaikin, and G. Schön, J. Low Temp. Phys. **106**, 305 (1997).
[11] See F. Giazotto, T. T. Heikkilä, A. Luukanen, A. M. Savin, and J. P. Pekola, Rev. Mod. Phys. **78**, 217 (2006), and references therein.
[12] The SQUID readout of the sensor can be multiplexed using standard SQUID multiplexing schemes, see, for example, T. M. Lanting, H.-M. Cho, J. Clarke, W. L. Holzapfel, A. T . Lee, M. Lueker, P. L. Richards, M. A. Dobbs, H. Spieler, and A. Smith, Appl. Phys. Lett. **86**, 112511 (2005).
[13] The expressions concerning the readout have been derived using the Josephson inductance model corresponding to the linearized current-phase relation. This allows for analytic expressions but slightly underestimates the detector response.
[14] M. Kiviranta, J. S. Penttilä, L. Grönberg, J. Hassel, A. Virtanen, and H. Seppä, Supercond. Sci. Technol. **17**, S285 (2004).
[15] F. Zhou, P. Charlat, B. Spivak, and B. Pannetier, J. Low Temp. Phys. **110**, 841 (1998).